JOURNAL OF MECHANICAL ENGINEERING AND SCIENCES
ISSN: 2289-4659 e-ISSN: 2231-8380
VOLUME 20, ISSUE 3, 2026, 12308 - 12321
DOI: https://doi.org/10.15282/jmes.20.3.2026.4.0881

RESEARCH ARTICLE

Experimental investigation and optimization of material removal rate and surface roughness in CNC plasma arc cutting of IS 2062 Gr B steel

Samir Chakravarti*, Nikki Shaw

Department of Mechanical Engineering, Kalyani Government Engineering College, Kalyani, 741235, West Bengal, India
Phone: + 91 (033) 25821309, Fax.: + 91 (033) 25821309

Abstract - This study experimentally analyzed the cutting behavior of IS 2062 Gr B steel using a computer numerical control plasma arc cutting (PAC) system. Several experiments were conducted to study the effect of the PAC key parameters, namely, the arc current, arc voltage, cutting speed, thickness of material, and pierce height, on the rates of material removal (MRR) and surface roughness (R_a). The Taguchi L18 orthogonal array was selected to design the experimental setup. The results showed that MRR was mostly affected by the thickness of the material and the arc current, while R_a was mostly influenced by material thickness, arc voltage, and cutting speed. Analysis of variance revealed that material thickness contributed 87.01% to the variation of MRR and 60.77% of R_a. The optimum parameter conditions for maximum MRR were 200 A arc current, 149 V arc voltage, 4500 mm/min cutting speed, 10 mm thickness, and 5.4 mm pierce height. The minimum R_a was found at the optimum conditions of 130 A arc current, 151 V arc voltage, 4500 mm/min cutting speed, 4 mm thickness, and 3 mm pierce height. The regression models developed for MRR and R_a were validated through 15 additional experiments, which showed close agreement with the predictions. To ensure excellent productivity and cut quality in industrial applications, this study offers experimentally validated settings for the PAC of IS 2062 Gr B steel.

Article History
Received : 16 December 2025
Revised : 11 February 2026
Accepted : 28 July 2026
Published : 30 September 2026

Keywords
Plasma arc cutting
Material removal rate
Surface roughness
Taguchi method
ANOVA
Optimization

1. Introduction

Plasma arc cutting (PAC) is a thermal cutting method that uses a narrow jet of high-temperature ionized plasma to melt and expel materials from a workpiece. It has become more prevalent in the industry because it can cut electrically conductive metals quickly, accurately, and with minimal post-processing [1]. PAC is used in manufacturing to produce complex profiles with minimal tool changes, thereby increasing production efficiency compared to conventional mechanical cutting [2]. PAC is commonly used for cutting metals in various industries, such as manufacturing, shipbuilding, railroad wagon, and machine fabrication [3]. PAC works by ionizing the cutting gas or plasma, producing a high-energy arc between the electrode and workpiece, and then focusing the energy on a small area by passing the plasma stream through a nozzle. Rapid heating and localized melting occur, and the force of the plasma jet causes the molten metal to be expelled, creating smaller heat-affected zones (HAZ) [4]. HAZ formation is crucial for preserving surface finish and structural integrity [5]- [6]. PAC cutting performance depends on process variables such as cutting speed, arc current, gas pressure, and standoff distance. Studies indicate that the heat input and, therefore, the HAZ, decrease with increasing cutting speed; however, the surface roughness can increase with excessive cutting speed [6]. Naganathan et al. [7] conducted an experimental study on plasma arc machining to investigate the effect of nickel nano-coated copper nozzles on surface roughness and machining efficiency. Dos Santos et al. [8] stated that holes made by PAC have a rougher surface than those made by helical milling, which affects tapping performance.

In this study, steel IS 2062 Gr. B was used as the workpiece, which is a low-carbon, hot-rolled structural steel used extensively in heavy engineering, construction, and industrial fabrication. It is highly valued for its wear resistance, high toughness, and ability to maintain mechanical strength at high temperatures, making it suitable for use in the petrochemical, oil and gas, and structural industries [9]. During welding, reduced carbide precipitation reduces the vulnerability to intergranular and localized corrosion [10]. Many other materials have been used by different researchers for PAC. Sonu and Singla [11] conducted experimental research on EN-45A material and optimized the plasma arc cutting process parameters. This study focused on EN-45A machinability to determine the effects of different process variables and the optimal conditions for the maximum material removal rate. According to Rzeźnikiewicz et al. [12], air plasma cutting is applicable to several building materials, such as copper, aluminum alloys, and high-strength steels. Hang et al. [13] tested CT3 steel of different thicknesses using a Bruco CNC plasma-cutting machine. Bhuvenesh et al. [14] conducted an experimental study on the plasma arc cutting of structural steel. Chamarthi et al. [15] studied the plasma arc cutting of Hardox-400 steel plates employing DoE to evaluate the surface unevenness caused by variations in the arc voltage, cutting speed, and plasma gas flow rate. ANOVA showed that the cut profiles varied with plate orientation, but the parameters improved the surface quality once optimized. Kumar [16] performed a factorial DOE and Taguchi-based optimization of PAC parameters for AISI 206 steel, emphasizing kerf width and penetration depth. Using optimization techniques such as Taguchi and ANOVA, Sharma et al. [17] verified that cutting speed, current, and gas pressure are significant factors influencing MRR.

However, research on the PAC machining of steel IS2062 Gr B remains limited despite its widespread industrial use. Recent studies indicate that further investigation is needed to quantify the influence of arc current, arc voltage, cutting

*CORRESPONDING AUTHOR | **Samir Chakravarti** | ✉ samir.chakravarti40@gmail.com
© 2026 The Authors. Published by Universiti Malaysia Pahang Al-Sultan Abdullah Press. This is an open access article under the CC BY-NC 4.0 license

speed, material thickness, and pierce height on MRR and surface roughness for IS2062 Gr B steel, as no prior research has addressed this topic [18]. Examining PAC performance on this material matters from both commercial and technical standpoints, given its economic significance and industrial use. The novel aspect of this study is that it addresses a research gap by examining IS 2062 Gr B material and systematically investigating how key PAC parameters, such as arc current, arc voltage, cutting speed, material thickness, and pierce height, affect MRR and Ra, both alone and in combination, using experimental and statistical methods. In this study, the experimental processes were set up with a Taguchi orthogonal array to capture the influence of several parameters effectively. In addition, ANOVA was used to determine the parameters that matter most, as well as the percentage share they give to MRR and Ra. To obtain a smaller Ra and a larger MRR, optimal parameter settings were identified, and then a few confirmatory experiments were conducted to validate the findings. An additional novelty of this work is that regression models for both MRR and Ra were constructed using experimental data and validated with an additional fifteen experiments to ensure predicted accuracy.

2. Materials and Methods

This section discusses the material specifications, experimental setup, and experimental design employed in this study.

2.1 Material Specifications

PAC is a thermal cutting process that removes material using a focused, high-speed stream of ionized gas, commonly known as plasma. The test specimen was made of IS 2062 Gr B steel. The alloy constituents of IS 2062 Gr B steel plates inherit several properties. However, the plates' strong durability, high ductility, stability at high temperatures, and capacity to withstand corrosion are some of its properties [9]. Tables 1, 2, and 3 present the material's chemical composition, mechanical properties, and thermal properties [18].

Table 1. Chemical composition of IS2062 Gr B steel

Grade Designation	Quality	Ladle Analysis, Maximum %					Carbon Equivalent (CE), Maximum %	Mode of Deoxidation
		C	Mn	S	P	Si		
2062	Gr B	0.22	1.50	0.045	0.045	0.40	0.41	Semi-killed /killed

The elements that constitute IS 2062 Gr B steel are sulfur (S), manganese (Mn), silicon (Si), phosphorus (P), and carbon (C). The carbon content is limited to a maximum of 0.22%, which helps maintain good weldability and reduces the risk of brittleness.

Table 2. Mechanical properties of IS2062 Gr B steel

Material	Yield strength (MPa)			Elongational (%)	Tensile strength (MPa)
	20 MPa - 40 MPa	<20 MPa	>40 MPa		
IS 2062 GR B	240	250	230	23	410

Manganese is present up to 1.50%, which improves strength and toughness without compromising ductility. The presence of sulfur (S) and phosphorus (P) is restricted to 0.045% each, as higher levels of these elements can lead to brittleness and reduced mechanical properties of the steel. Additionally, silicon may be present up to 0.40%, contributing to increased strength and improving the steel's ability to withstand deformations.

Table 3. Thermal properties of IS 2062 Gr B steel

Thermal properties of IS 2062 Gr B	Value
Density	8000 Kg/m³
Coefficient of thermal expansion	0.000013/°C
Thermal conductivity	0.032 kW/m°C
Specific heat	481.000 J/Kg°C

2.2 Experimental Setup

Initially, 300 × 500 mm rectangular parent plates with 4 mm, 6 mm, and 10 mm thicknesses were utilized. Using the PAC method, smaller test specimens measuring 80 × 80 mm and with the same thicknesses were created from these plates to conduct the experiments. Figure 1 depicts the Computer Numerical Control (CNC) MAXPRO200 plasma arc cutting machine used for the experiments. The power supply maintains a steady current by adjusting the voltage as needed. The high-frequency starter generates a quick pulse to ionize the gas and initiate the arc. The cathode, or negative electrode, is located inside the nozzle of the torch through which the gas passes. Excessive energy is gained by the gas as it is forced through a small nozzle opening, changing into plasma and cutting the metal. During the cutting operation, the torch moves over the workpiece, while the workpiece remains stationary, as shown in Figure 1. Table 4 lists the essential operational features and capabilities of the plasma arc cutting machine.

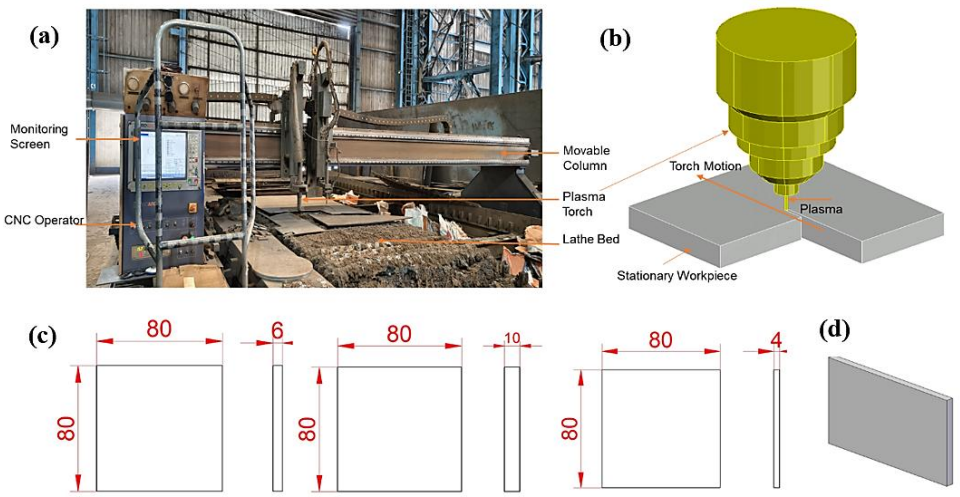


Figure 1. (a) CNC plasma arc cutting machine, (b) CAD design showing the torch movement direction, (c) Specimen dimensions for thicknesses of 4 mm, 6 mm, and 10 mm, (d) 3D design of specimen

Table 4. Specifications of CNC plasma arc cutting machine

Parameter	Value
Maximum open circuit voltage	360 VDC
Maximum output current	200 A
Output voltage	50 – 160 VDC
Duty cycle rating	100% @33 kW, 40° C
Ambient temperature	-10° C to +40° C
Power factor	0.98 @ 33 kW output
Cooling	Forced Air (Class F)
Insulation	Class H

The equipment comprised major parts such as the CNC operator, monitoring screen, movable column, power supply, plasma torch, lathe bed, electrode, nozzle, and cutting table. The torch position is kept vertical with respect to the workpiece. The maximum production capacity is the maximum thickness that can be cut at 100% duty cycle. Compressed air is commonly utilized as the cutting gas, simplifying and reducing the cost of the process. In this work, air was employed as both the primary plasma gas and the secondary shielding gas. The nozzle assembly of a plasma arc machine torch is made up of several parts. These consist of the shield cap, nozzle, swirl ring, electrode, and nozzle retaining cap. It is crucial that the various components of the plasma torch are assembled properly. Each component contributes to the plasma arc's formation and direction, enabling the torch to precisely and correctly cut through any metal [19]. In PAC, several process parameters are crucial in determining the quality and efficiency of the cut. The amount of electrical energy required to create the plasma arc is controlled by the arc current, which is expressed in amperes (A). Arc voltage (V) can assist in maintaining a stable arc and yield a smoother cut, but if the voltage is excessively high, it may cause the arc to become unstable [10]. Cutting speed is another important element; it relates to the speed at which the torch moves across the material. Material thickness is the depth of the workpiece being cut. Pierce height is the initial distance between the workpiece and the torch at the beginning of the cut. The selection of appropriate process factors and their impact on part quality evaluation are essential for improving PAC's cutting quality and performance characteristics [20].

Thirty-three experiments were conducted in this study to explore MRR and R_a under different parameter conditions, with two confirmation experiments conducted. Figure 2 shows image views of the 33 experiments, with the experiment numbers labeled individually. The specimen models were initially created using AutoCAD. The AutoCAD drawing was then loaded into OmniCAD for nesting, which resulted in a more efficient cutting process. Nesting in CNC is the technique of arranging components on a material sheet to reduce waste and increase efficiency. Once the drawing was properly nested, it was transferred into the plasma arc CNC controller, and the machine was ready to cut after a thorough inspection. The duration of each experiment was recorded using a stopwatch. The material removal rate is an essential measure that quantifies the amount of material removed per unit of time during machining [21]. Roughness is often also a good indicator for the performance of a mechanical component because surface imperfections can act as sites for nucleation of corrosion or cracks [22]. In this work, the average surface roughness was measured. The average roughness can be defined as the integral of the absolute value of the roughness profile height over the length. A dial indicator was used to measure the surface roughness. This study involved 18 experiments utilizing the Taguchi L18 orthogonal array for model development and analysis, alongside an additional 15 experiments conducted independently to validate the regression models.

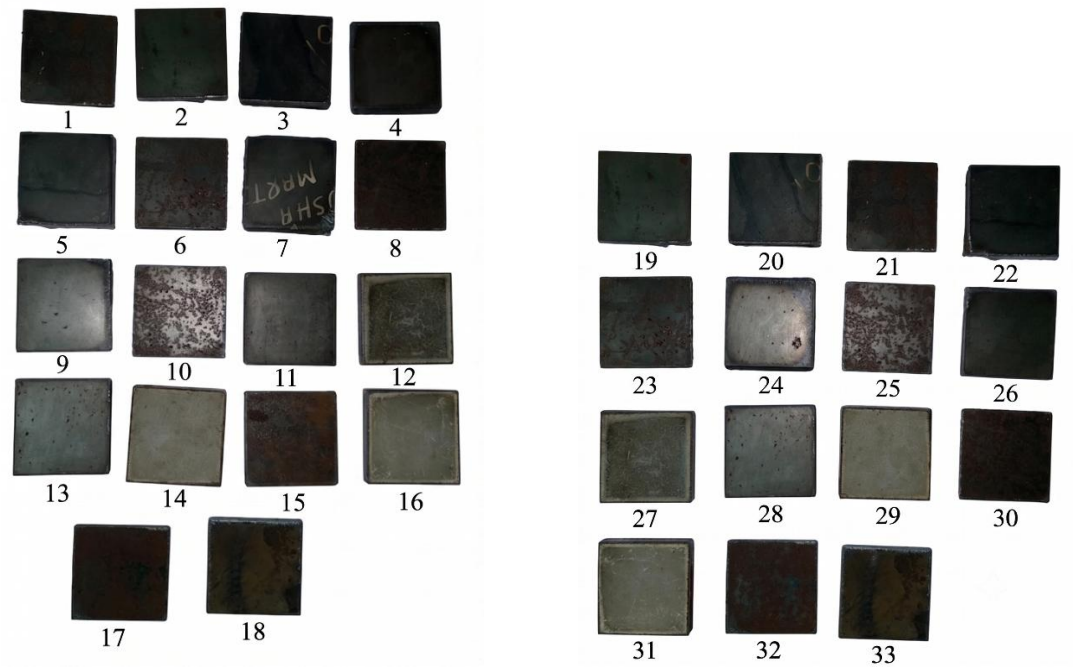


Figure 2. Image views of thirty-three experiments with each experiment numbered sequentially

2.3 Design of Experiment

Design of Experiment (DoE) is a statistical method that deals with planning, conducting, analyzing, and interpreting experiments to determine how different factors affect process performance and find the best values for those variables [23]. The whole analysis was centered around five factors: arc current, arc voltage, cutting speed, material thickness, and pierce height. The factor with different levels is shown in Table 5. The arc current was varied between two values: 130 A and 200 A. Three levels of arc voltage adjustment (147, 149, and 151 V) were used to determine how variations in arc energy affected the cut. Three distinct values, which correspond to slow to fast torch movement, were chosen for the cutting speed: 3500 mm/min, 4000 mm/min, and 4500 mm/min. Metal plates with thicknesses of 4 mm, 6 mm, and 10 mm were employed in the experiment to ensure a range of workpieces from extremely thin to moderately thick. Lastly, three different values for the pierce height were taken: 3.0 mm, 4.2 mm, and 5.4 mm. These specific parameter values allowed for a systematic investigation into how each factor contributes to cutting quality and efficiency.

Table 5. Factors and their levels used in the experimental design

Factor	Level 1	Level 2	Level 3
Arc current, I_a (A)	130	200	–
Arc Voltage, V_a (V)	147	149	151
Cutting speed, v_c	3500	4000	4500
Material thickness, t_m	4.0	6.0	10.0
Pierce height, h_p (mm)	3.0	4.2	5.4

The Taguchi method uses orthogonal arrays (OAs) to design experiments in a systematic manner, while accounting for the influence of several process parameters on the output. The challenging part is selecting the appropriate OA, which is mostly determined by the total DOF, which is calculated as the count of factors plus the number of levels each factor has. In this experimental setup, four factors were at three levels and one factor was at two levels; therefore, the overall DOF was 9, calculated as factors × (number of factor levels – 1) [23]. The OA was determined such that its DOF was either equal to or greater than that of the operation parameters. To accommodate this, the L18 ($2^1 \times 3^4$) orthogonal array was selected, as it supports one 2-level factor and up to seven 3-level factors. The influence of all these factors on the performance characteristics was controlled by the signal-to-noise (S/N) ratio [24]. The S/N ratio for the larger-the-better case can be calculated using Eq. (1), where Eq. (2) is used for the smaller-the-better situation [23].

$$S/N = -10\,log(\sum \frac{1}{n}(1/y^2)) \quad (1)$$

$$S/N = -10\,log(\sum \frac{1}{n}(y^2)) \quad (2)$$

where, response is *y* and *n* are the number of observations made for each run, and the value is 1. The optimal value and percent significance of each parameter were calculated using ANOVA. Using the optimum set of parameters, Eq. 3 gives the expected S/N [23].

$$(S/N)_p = \overline{(S/N)} + \sum_{i=1}^{m} ((S/N)_i - \overline{(S/N)}) \quad (3)$$

where, $\overline{(S/N)}$, $(S/N)_p$, and $(S/N)_i$ are the mean, predicted, and optimum S/N ratio respectively. m is equal to the number of control factors.

3. Results and Discussion

Initially, 18 experiments were conducted, with five key variables: cutting speed, arc voltage, arc current, material thickness, and pierce height. For each experiment, the MRR and R_a were calculated. Tables 6 and 8 present the full configuration of every experimental setup, together with the corresponding outcomes. Furthermore, for each experimental run, the S/N ratio was calculated for both MRR and R_a; the findings are displayed in Tables 6 and 8, respectively. To ascertain the impact of each factor level on the performance metrics, average S/N ratios were computed. The impacts of these averages on MRR and R_a are shown in Figure 4 and Figure 5, respectively. Table 7 shows the corresponding values of response for S/N ratios, which highlight the impacts of the level of every factor. The analysis of the findings was performed at a significance level of 0.05.

Table 6. Experimental findings and S/N ratios for MRR with varied arc current, arc voltage, cutting speed, material thickness, and pierce height

Exp. No	I_a (A)	V_a (V)	v_c (mm/min)	t_m (mm)	h_p (mm)	MRR (mm^3/s)	S/N for MRR
1	130	147	3500	4	3	2987.16	69.51
2	130	147	4000	6	4.2	3779.53	71.55
3	130	147	4500	10	5.4	5169.63	74.27
4	130	149	3500	4	4.2	2962.96	69.43
5	130	149	4000	6	5.4	3930.40	71.89
6	130	149	4500	10	3	5120.00	74.19
7	130	151	3500	6	3	3954.69	71.94
8	130	151	4000	10	4.2	5311.20	74.50
9	130	151	4500	4	5.4	3137.25	69.93
10	200	147	3500	10	5.4	5284.89	74.46
11	200	147	4000	4	3	3212.05	70.14
12	200	147	4500	6	4.2	5013.05	74.00
13	200	149	3500	6	5.4	4794.01	73.61
14	200	149	4000	10	3	5776.17	75.23
15	200	149	4500	4	4.2	3531.03	70.96
16	200	151	3500	10	4.2	5067.30	74.10
17	200	151	4000	4	5.4	3316.06	70.41
18	200	151	4500	6	3	4705.88	73.45

3.1 Effect of Different Parameters on MRR

The main effects plot for the S/N ratios (Figure 3) describes the effect of the process parameter on the MRR, taking the larger-is-better criterion. The parameters can be ranked according to their effect on the S/N ratio. The arc current is an important factor influencing the S/N ratio. The mean S/N ratio increased with an increase in the arc current from 130 A to 200 A. The higher the arc current, the more energy delivered to the plasma, thereby improving the thermal efficiency of the cutting process [25]. The thickness of the material is another major parameter influencing the MRR. As the thickness increased from 4 mm to 10 mm, there was a steep increase in the S/N ratio. A thicker material favors longer arc contact and subsequently increases the MRR with better energy transfer from the plasma to the material [26]. The S/N ratio is moderately impacted by the cutting speed. The S/N ratio improves slightly but steadily as the cutting speed increases from 3500 mm/min to 4500 mm/min. In plasma arc cutting, higher cutting speeds help with faster machining and consequently, higher rates of material removal. However, they also cause a major decline in surface roughness or machining quality [27].

Table 7. Response table for ratios of S/N with rank and difference of S/N for MRR and Ra for three different levels of variables- arc current, arc voltage, cutting speed, material thickness, and pierce height

Level	MRR					R_a				
	I_a	V_a	v_c	t_m	h_p	I_a	V_a	v_c	t_m	h_p
1	71.91	72.32	72.18	70.06	72.41	-25.87	-26.65	-26.73	-24.93	-26.01
2	72.93	72.55	72.29	72.74	72.42	-26.38	-26.27	-25.96	-26.09	-26.14
3		72.39	72.80	74.46	72.43		-25.45	-25.68	-27.35	-26.23
Delta	1.02	0.23	0.62	4.40	0.02	0.51	1.20	1.05	2.42	0.22
Rank	2	4	3	1	5	4	2	3	1	5

The arc voltage showed a slight variation in the SN ratio. From 147 to 149 V, the SN ratio slightly increased, and at 151 V, it slightly decreased. This suggests that during plasma arc cutting, MRR first improved with a moderate increase in arc voltage. But MRR decreases after a certain voltage. In a related study, Bhuvenesh et al. [14] discovered that when using a manual plasma arc cutting machine to cut standard AISI 1017 steel, MRR first improved with a moderate increase in arc voltage but decreased as the voltage increased further. The energy density was sufficiently high to efficiently melt and expel the material at moderate arc voltages, thereby increasing MRR [20]. The workpiece is more likely to overheat as the voltage increases above a specific level, which could result in excessive melting instead of effective cutting [25].

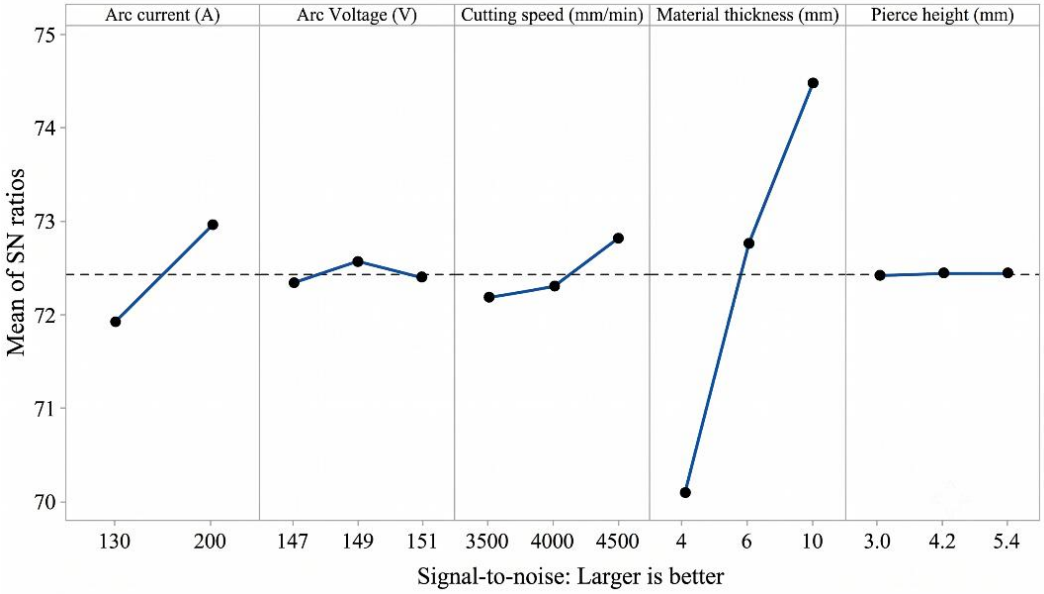


Figure 3. The average S/N ratio behaviour for MRR for three different levels of variables: cutting speed, arc voltage, arc current, material thickness, and pierce height

The S/N ratio showed no noticeable change with the pierce height because the curve remained mostly flat. This indicates that changes in the pierce height within the studied range did not affect the MRR. This is because the pierce height primarily affects the initial penetration and piercing quality, not the steady-state cutting process. Once cutting starts, the height has little effect on the energy used or heat transferred in the cutting zone. Although it does not directly correlate with the MRR, maintaining a constant pierce height is crucial for optimal cutting performance. Research has shown that changes in cutting speed and arc current have a greater impact on MRR than adjustments to pierce height [28]. The S/N ratio analysis (Table 7 and Figure 3) for MRR shows that the material thickness is the most important parameter. The other parameters, in order, were arc current, cutting speed, arc voltage, and piercing height, the least important.

3.2 Effect of Different Parameters on Surface Roughness

Using the smaller-the-better criterion, the main effects plot for the S/N ratios (Figure 4) shows how each process parameter affects the surface roughness. A higher mean S/N ratio, which corresponds to a lower surface roughness, is produced by a lower current (130 A). The R_a slightly increased as the arc current increased from 130 A to 200 A. Higher arc currents can cause more heat to enter the cutting area, which may make cutting more efficient but also make the surface rougher because of excessive melting and oxidation [29-30]. However, increasing the arc voltage from 147 V to 151 V makes the surface less rough. A higher arc voltage makes the arc more stable and maintains more stable cutting conditions, which can make the surface smoother [14]. R_a moderately decreases as the cutting speed increases from 3500 mm/min to 4500 mm/min. This is because faster speeds minimize the heat-affected zones and shorten the duration of heat exposure per unit length, resulting in smoother and cleaner surfaces. According to a recent study, higher cutting speeds typically yield smoother surfaces, whereas lower speeds typically result in higher R_a values [31].

Table 8. Experimental findings and S/N ratios for R_a with varied arc current, arc voltage, cutting speed, material thickness, and pierce height

Exp. No	I_a (A)	V_a (V)	v_c (mm/min)	t_m (mm)	h_p (mm)	R_a (µm)	S/N for R_a
1	130	147	3500	4	3	19.845	-25.95
2	130	147	4000	6	4.2	21.315	-26.57
3	130	147	4500	10	5.4	22.867	-27.18
4	130	149	3500	4	4.2	18.872	-25.52
5	130	149	4000	6	5.4	20.432	-26.21
6	130	149	4500	10	3	21.748	-26.75
7	130	151	3500	6	3	17.940	-25.08
8	130	151	4000	10	4.2	19.638	-25.86
9	130	151	4500	4	5.4	15.306	-23.70
10	200	147	3500	10	5.4	27.692	-28.85
11	200	147	4000	4	3	18.278	-25.24
12	200	147	4500	6	4.2	20.224	-26.12
13	200	149	3500	6	5.4	22.289	-26.96
14	200	149	4000	10	3	23.547	-27.44
15	200	149	4500	4	4.2	17.246	-24.73
16	200	151	3500	10	4.2	25.236	-28.04
17	200	151	4000	4	5.4	16.712	-24.46
18	200	151	4500	6	3	19.030	-25.59

Increasing the thickness of the material from 4 mm to 10 mm makes the surface much rougher. When materials are thicker, they hold more heat and cool down more slowly. This makes the heat-affected zones larger and the melting and solidification patterns less regular. This makes the cut surface rougher. Bhuvenesh et al. [14] also found that thicker materials can make surface irregularities more noticeable, which is detrimental to the surface quality. The pierce height has a negligible impact on R_a. However, the R_a tends to increase slightly as the pierce height increases from 3.0 mm to 5.4 mm. When the torch is farther away from the material surface, there may be less effective initial penetration and more arc instability, which makes the surface rougher. The S/N ratio analysis (Table 7 and Figure 4) for surface roughness shows that the most important parameter is the material thickness, followed by the arc voltage, cutting speed, arc current, and pierce height, which is the least important.

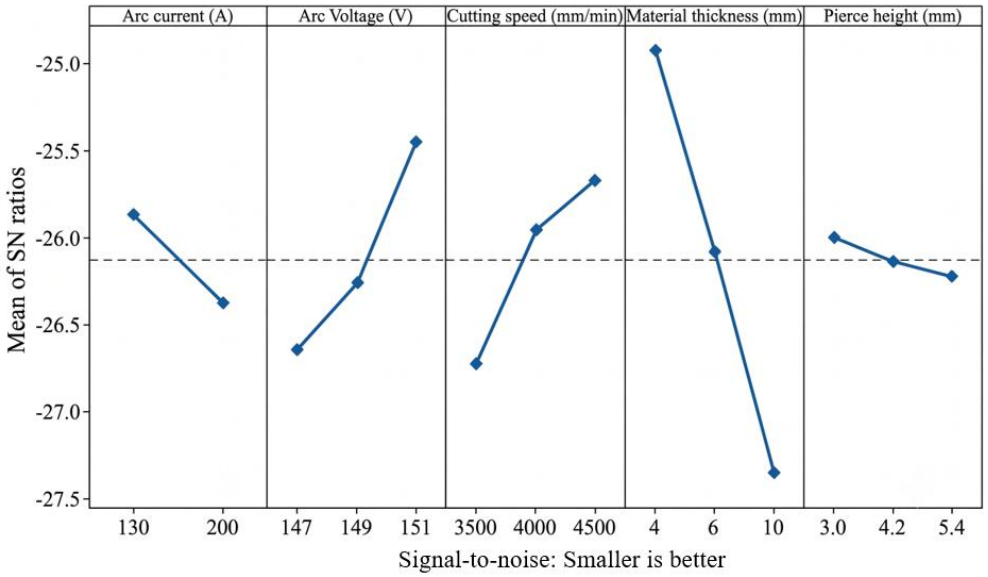


Figure 4. The average S/N ratio behaviour for R_a for three different levels of variables: cutting speed, arc voltage, arc current, material thickness, and pierce height

3.3 Optimization of the MRR and R_a

After assessing the effect of various parameters on MRR and R_a, the percentage contribution of each parameter was computed, and their values were optimized. The ANOVA method (Table 9) was used to calculate the percentage of the total contribution of each parameter. The F-measure in ANOVA is a useful statistic for measuring the importance of differences in group means. According to the ANOVA results for MRR, the most important factor was the material thickness, which had a low P-value of 0.006 (<0.05), a very high F-value of 84.46, and a contribution of 87.01%. With a 6.90% contribution, an F-value of 13.38, and a low P-value of 0.006, arc current is the next significant parameter that has

a statistically significant effect on MRR. The low contribution percentages and high P-values (>0.05) of cutting speed (C = 1.66%, P = 0.259), arc voltage (C = 0.31%, P = 0.752), and pierce height (C = 0.01%, P = 0.991) on the other hand, suggest that they have little effect on the variation in MRR within the tested ranges.

Table 9. The ANOVA findings for MRR and R_a display parameters: process parameters- PPS, sum of squares- SoS -, adjusted-Adj -, mean square- M.S -, degrees of freedom- DoF, contribution-C, and statistical significance- P

P. P	DF	C (%)	Adj SS	Adj MS	F-Value	P-Value
I_a	1	6.90	1,050,101	1,050,101	13.38	0.006 (Significant)
V_a	2	0.31	46,435	23,217	0.30	0.752 (Not Significant)
v_c	2	1.66	252,504	126,252	1.61	0.259 (Not Significant)
t_m	2	87.01	13,254,426	6,627,213	84.46	<0.001 (Significant)
h_p	2	0.01	1,369	684	0.01	0.991 (Not Significant)
Error	8	4.12	627,753	78,469		
Total	17	100	15,232,587			
I_a	1	5.12	8.393	8.393	7.27	0.027 (Significant)
V_a	2	13.90	22.788	11.394	9.87	0.007 (Significant)
v_c	2	13.35	21.883	10.942	9.48	0.008 (Significant)
t_m	2	60.77	99.579	49.789	43.12	<0.001 (Significant)
h_p	2	1.23	2.020	1.010	0.87	0.453 (Not Significant)
Error	8	5.63	9.237	1.155		
Total	17	100	163.900			

Overall, material thickness was the most dominant factor affecting MRR, contributing the highest percentage of variation, followed by arc current, which also exhibited a significant influence. Table 7 and the S/N diagram (Figure 3) show that the optimal parameter setup for maximizing MRR is $I_{a2}V_{a2}v_{c3}t_{m3}h_{p3}$. If the material thickness was a constraint (fixed at 10 mm), the best process settings for achieving a high MRR were an arc current of level 2 (200 A), an arc voltage of level 2 (149 V), a cutting speed of level 3 (4500 mm/min), and a pierce height of level 3 (5.4 mm). According to the surface roughness ANOVA results (Table 9), material thickness was the most important factor, accounting for 60.77% of the total variation. Strong statistical significance was confirmed by the extremely high F-value of 43.12 and the extremely low P-value of 0.000. With respective contributions of 13.90% and 13.35%, arc voltage and cutting speed were also significant. Their P-values were well below 0.05, suggesting that variations in these parameters also significantly affected R_a. At a contribution of 5.12% and a P-value of 0.027 (<0.05), arc current accounted for a smaller but statistically significant amount of the variation. With a low contribution of 1.23% and a high P-value of 0.453 (>0.05), Pierce height was not statistically significant in connection to R_a. Overall, Pierce height had a minor impact on surface roughness, while material thickness was the most important factor, followed by arc voltage, cutting speed, and arc current. According to the S/N ratios (Figure 4) and response table (Table 7), $I_{a1}V_{a3}v_{c3}t_{m1}h_{p1}$ was the optimum parameter combination for reducing R_a. The optimum conditions for the lowest R_a were an arc current at level 1 (130 A), arc voltage at level 3 (151 V), cutting speed at level 3 (4500 mm/min), material thickness at level 1 (4 mm), and pierce height at level 1 (3 mm).

3.4 Optimal Value

The ANOVA approach considers the significant levels of the process parameters to forecast the optimal value of the performance characteristics, that is, MRR and R_a. Using Eq. (3), the optimal S/N ratio values for the corresponding process parameters were determined. Table 10 shows $\overline{(S/N)}$ value, ratio of S/N at the optimal parameter level [$(S/N)_{I_a}$, $(S/N)_{V_a}$, $(S/N)_{v_c}$, $(S/N)_{t_m}$, and $(S/N)_{h_p}$] obtained from Tables 6-8, respectively.

Table 10. Ratio of S/N at the optimal parameter level and mean S/N ratio values for MRR and R_a

Output	$\overline{(S/N)}$	$(S/N)_{I_a}$	$(S/N)_{V_a}$	$(S/N)_{v_c}$	$(S/N)_{t_m}$	$(S/N)_{h_p}$
MRR	72.76	72.93	72.55	72.80	74.46	72.43
R_a	-25.69	-25.87	-25.45	-25.68	-24.93	-26.01

Finally, the MRR and R_a at the optimal level were obtained from Eq. 1 and Eq. 2, respectively. Table 11 lists the optimal predicted values for the performance characteristics.

3.5 Confirmation Test

Once the optimal levels of process variables have been determined, a validation experimental test must be performed to Once the best levels of the process variables were worked out, there should be a validation experimental test to make sure the Taguchi and ANOVA analyses are actually correct in practice. To strengthen the findings, two types of confirmation tests were conducted using the optimum factor settings, one addressing MRR and the other addressing Ra. Table 11 shows

the predicted values side by side with the confirmatory experiments conducted. The fact that the confirmation results have such a low percentage error proves that the analyses are accurate.

Table 11. Comparison of confirmatory mean and predicted values with error % for MRR and R_a

Output characteristics	Optimum combination of parameters	Confirmatory Mean value	Predicted Value	Error (%)
MRR	$I_{a2}V_{a2}v_{c3}t_{m3}h_{p3}$	5082.91	5270.64	3.64
R_a	$I_{a1}V_{a3}v_{c3}t_{m1}h_{p1}$	18.18	19.09	4.75

3.6 Regression Analysis

Regression analysis is a statistical method that checks how variables relate and then tries to determine the most suitable fitted model for forecasts or practical solutions [23]. Here, the present work put together a multiple linear regression model, and it did that with the experimental information listed in Tables 6 and 8, using both the input factors and the output findings from the experimental process. Table 12 shows the values for R^2, R^2 (adjusted), and R^2 (predicted) obtained by the model.

Table 12. R^2, R^2 (adjusted), and R^2 (predicted) results for the MRR and R_a regression equations

Regression	R^2	R^2 (predicted)	R^2 (adjusted)
MRR	95.88%	91.24%	79.14%
R_a	92.06%	88.75%	82.17%

For each MRR and Ra, the high R^2, R^2 (adjusted), and R^2 (predicted) results indicate that the models were precise, predictive, and well-suited to the data. Equations 4 and 5 are the regression equations for the MRR and R_a models, respectively:

$$MMR = -409 + 6.90I_a + 1.9V_a + 0.271v_c + 332.6t_m - 8.6h_p \quad (4)$$

$$R_a = 121.4 + 0.01951I_a - 0.682V_a - 0.002575v_c + 0.9368t_m + 0.341h_p \quad (5)$$

The regression models (Eqs. 4 and 5) are straight lines. The main effects plot for Arc Voltage (Figure 3) shows a trend that is not linear (it goes up and then down). The linear regression model provides a good idea of the overall trend of the data, but it cannot mathematically recreate the inflection point that was observed at 149 V. First, the created models were compared to the experimental record (Tables 6 and 8 for MRR and Ra, respectively, Exp. At first, the created models were compared to the experimental record (Table 6 for MRR and Table 8 for Ra, Exp. No. 1-18). Second, run the regression model on a new set of experimental data (Exp. No. 19-33). This sort of validation helps to show the real-world usefulness or practical applicability of the current regression model when it meets new data. After that, Table 13 and Table 14 present, side by side, the results comparing the measured values with the estimated MRR and R_a produced by the regression model. Here, these comparisons are shown for the first and second validation situations, respectively. The visual representations of the thirty-three experiments are also depicted in Figure 2.

To gauge the accuracy of the regression model, the absolute error was calculated in every run. This is the percentage difference between what was found experimentally and what was expected theoretically, that is, from the regression equations. Thirty-three experimental data points were used to validate the MRR regression model (Table 13). The findings (Table 13) demonstrate that the model produces extremely accurate predictions for the initial dataset (experiments 1–18), with error percentages generally falling within a small range, usually less than 5%, with some cases as low as 0.13%. This validates the accuracy of the model during development. The regression model continued to perform effectively during the extended validation with the additional 15 testing points (experiments 19-33), with the majority of prediction errors remaining below 10%. Two cases showed errors of more than 10%. However, the overall prediction performance was consistent and acceptable for practical applications.

Similarly, the first 18 experimental data points were used to build the regression model for R_a, and the remaining 15 experiments were used to test the model's predictive ability in addition to retesting the first 18 samples, as shown in Table 14. The error percentage (Table 14) for the initial dataset (Exp. No. 1-18) was largely within a reasonable range, usually less than 10%, with many values around 1–5%, indicating a strong model fit. For example, experiments 1, 3, 4, and 10 had extremely low errors of 2.04%, 1.91%, 2.05%, and 1.61%, respectively. This implies that the model accurately captured the effect of process variables on R_a during model building. For the additional testing data (Exp. No. 19–33), the model's predictions were strongly accurate for multiple runs, including Exp. No. 19 (0.51% error) and Exp. No. 21 (1.36% error), indicating the model's overall validity. However, three cases had errors of more than 10%. Overall, the model showed good surface roughness prediction ability, with the majority of errors being reasonably small. The regression model's graphical presentation for MRR and R_a is displayed in Figure 5, along with the experimental values used to validate the model. Figure 5 demonstrates how closely the output predicted by the regression model matches the output observed experimentally. This suggests that the MRR and R_a regression formulae are highly precise.

Table 13. Error percentage, or the difference between regression-predicted values and experimental data for MRR

Exp. No.	I_a (A)	V_a (V)	v_c (mm/min)	t_m (mm)	h_p (mm)	MRR from Experiment (mm^3/s)	MRR from Regression Eq. (mm^3/s)	Error (%)
1	130	147	3500	4	3	2987.16	3020.40	1.11
2	130	147	4000	6	4.2	3779.53	3810.78	0.83
3	130	147	4500	10	5.4	5169.63	5266.36	1.87
4	130	149	3500	4	4.2	2962.96	3013.88	1.72
5	130	149	4000	6	5.4	3930.40	3804.26	3.21
6	130	149	4500	10	3	5120.00	5290.80	3.34
7	130	151	3500	6	3	3954.69	3693.20	6.61
8	130	151	4000	10	4.2	5311.20	5148.78	3.06
9	130	151	4500	4	5.4	3137.25	3278.36	4.50
10	200	147	3500	10	5.4	5284.89	5478.36	3.66
11	200	147	4000	4	3	3212.05	3638.90	13.29
12	200	147	4500	6	4.2	5013.05	4429.28	11.65
13	200	149	3500	6	5.4	4794.01	4151.76	13.40
14	200	149	4000	10	3	5776.17	5638.30	2.39
15	200	149	4500	4	4.2	3531.03	3767.88	6.71
16	200	151	3500	10	4.2	5067.30	5496.28	8.47
17	200	151	4000	4	5.4	3316.06	3625.86	9.34
18	200	151	4500	6	3	4705.88	4447.20	5.50
19	130	149	3500	6	5.4	3410.30	3668.76	7.58
20	130	149	4000	10	3	5148.83	5155.30	0.13
21	130	149	4500	4	4.2	3324.68	3284.88	1.20
22	130	151	3500	10	4.2	4855.84	5013.28	3.24
23	130	151	4000	4	5.4	3417.89	3142.86	8.05
24	130	151	4500	6	3	4137.93	3964.20	4.20
25	200	147	3500	4	4.2	2895.93	3493.08	20.62
26	200	147	4000	6	5.4	4388.57	4283.46	2.40
27	200	147	4500	10	3	5087.44	5770.00	13.42
28	200	149	3500	6	3	4512.34	4172.40	7.53
29	200	149	4000	10	4.2	5745.06	5627.98	2.04
30	200	149	4500	4	5.4	3770.25	3757.56	0.34
31	200	151	3500	10	5.4	4945.90	5485.96	10.92
32	200	151	4000	4	3	3436.24	3646.50	6.12
33	200	151	4500	6	4.2	4324.32	4436.88	2.60

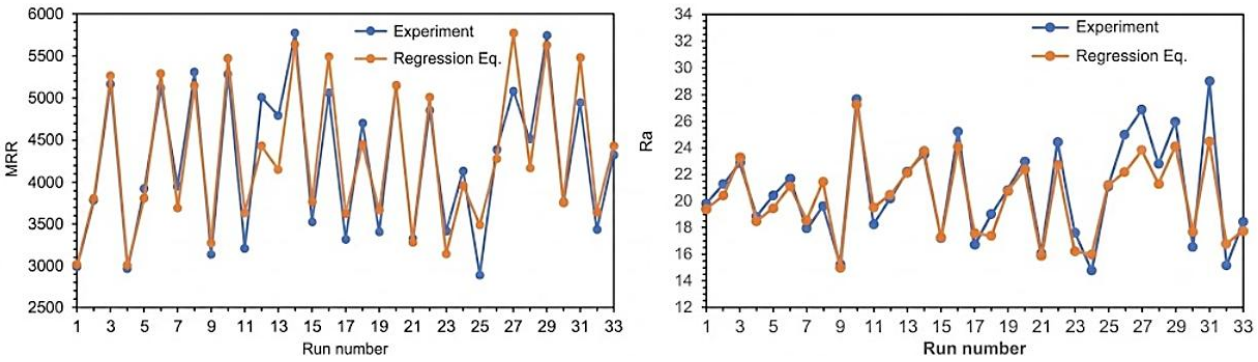


Figure 5. Comparison of MRR and R_a between findings from experiments and the regression model for different run numbers

Table 14. Error percentage, or the difference between regression-predicted values and experimental data for R_a

Exp. No	I_a (A)	V_a (V)	v_c (mm/min)	t_m (mm)	h_p (mm)	R_a from Experiment (µm)	R_a from Regression Eq. (µm)	Error (%)
1	130	147	3500	4	3	19.845	19.440	2.04
2	130	147	4000	6	4.2	21.315	20.435	4.13
3	130	147	4500	10	5.4	22.867	23.304	1.91
4	130	149	3500	4	4.2	18.872	18.485	2.05
5	130	149	4000	6	5.4	20.432	19.481	4.66
6	130	149	4500	10	3	21.748	21.122	2.88
7	130	151	3500	6	3	17.940	18.586	3.60
8	130	151	4000	10	4.2	19.638	21.455	9.25
9	130	151	4500	4	5.4	15.306	14.955	2.29
10	200	147	3500	10	5.4	27.692	27.245	1.61
11	200	147	4000	4	3	18.278	19.518	6.79
12	200	147	4500	6	4.2	20.224	20.514	1.43
13	200	149	3500	6	5.4	22.289	22.134	0.70
14	200	149	4000	10	3	23.547	23.775	0.97
15	200	149	4500	4	4.2	17.246	17.276	0.17
16	200	151	3500	10	4.2	25.236	24.108	4.47
17	200	151	4000	4	5.4	16.712	17.609	5.37
18	200	151	4500	6	3	19.030	17.376	8.69
19	130	149	3500	6	5.4	20.875	20.768	0.51
20	130	149	4000	10	3	23.018	22.409	2.64
21	130	149	4500	4	4.2	16.130	15.910	1.36
22	130	151	3500	10	4.2	24.470	22.742	7.06
23	130	151	4000	4	5.4	17.653	16.243	7.99
24	130	151	4500	6	3	14.765	16.011	8.44
25	200	147	3500	4	4.2	21.111	21.215	0.49
26	200	147	4000	6	5.4	24.981	22.210	11.09
27	200	147	4500	10	3	26.876	23.852	11.25
28	200	149	3500	6	3	22.801	21.315	6.52
29	200	149	4000	10	4.2	25.973	24.184	6.89
30	200	149	4500	4	5.4	16.580	17.685	6.67
31	200	151	3500	10	5.4	29.001	24.517	15.46
32	200	151	4000	4	3	15.132	16.790	10.96
33	200	151	4500	6	4.2	18.506	17.786	3.89

4. Conclusions

The effects of important PAC parameters, such as the arc current, arc voltage, cutting speed, material thickness, and pierce height, on the MRR and R_a during machining of IS 2062 Gr B steel were studied in this research. The evaluation of the performance of PAC on this material is of both technical and commercial importance, as this material is used industrially on a large scale and is of economic importance. The study used the Taguchi method, ANOVA, and regression modelling for the optimization of the cutting process and to provide a comprehensive understanding of the parameter interactions. The experimental work was performed in a CNC plasma arc cutting machine to study the MRR and R_a with variations in parameters. The S/N analysis for MRR shows that the most important parameter is material thickness, followed by arc current, cutting speed, arc voltage, and pierce height, which is the least important. Cutting speed exhibited a moderate but consistent positive effect on MRR, and the MRR increased sharply with increasing thickness and higher arc current. While the pierce height had little effect because the S/N curve remained almost flat. In addition, it was observed that the MRR initially increased with arc voltage but then decreased. The ANOVA results indicate that the material thickness had the maximum effect on MRR, followed by the arc current, whereas the effects of arc voltage, cutting speed, and pierce height were relatively insignificant. The optimal condition for maximizing MRR was obtained at 200 A arc current, 149 V arc voltage, 4500 mm/min cutting speed, 10 mm thickness, and 5.4 mm pierce height. For surface roughness, greater material thickness resulted in a significantly rougher surface. R_a increased slightly with higher arc current and moderately decreased as the cutting speed increased. Although the pierce height had little effect, R_a tended to increase slightly at higher values of pierce height. Higher arc voltages reduced surface roughness. The S/N ratio analysis of R_a indicated that the material thickness was the most significant factor, followed by arc voltage, cutting speed, and arc current, and the least significant factor was pierce height. The analysis of variance for R_a showed that the material thickness had the most significant effect on R_a, followed by arc voltage, cutting speed, and arc current, and pierce height had a negligible effect.

The optimal parameter combinations for reducing Ra were 130 A arc current, 151 V arc voltage, 4500 mm/min cutting speed, 4 mm thickness, and 3.0 mm pierce height. The optimum parameters for reduced Ra and increased MRR were successfully determined using the Taguchi and ANOVA methods. The optimum parameter settings were used in the confirmation tests, one for MRR and the other for R_a. The confirmatory results of tests with an error of a low percentage are indicative of analysis accuracy. The regression models created for MRR and R_a are highly accurate in prediction. Further validation of the regression models was done by fifteen additional experiments, with prediction errors mostly less than 5%.

Overall, the current study addresses a critical material of industrial importance, IS 2062 Gr B steel, and highlights the potential for process parameter optimisation of PAC operations to enhance the quality (low Ra) and productivity (high MRR). The results are directly applicable to the petrochemical, oil and gas, and structural industries that use IS 2062 Gr B. For wider applicability, future studies could include other materials and plasma gases for analysis.

Acknowledgments
The experimental work described in this study was conducted at Sarralle Equipment India Pvt. Ltd., West Bengal, 711303. The authors would like to thank the technical and supervisor team of Sarralle Equipment India Pvt. Ltd., West Bengal,711303.

Funding
This research did not receive any specific grant from funding agencies in the public, commercial, or not-for-profit sectors

Declaration of Competing Interest
The authors declare no conflict of interest.

CRediT Authorship Contribution Statement
S. Chakravarti: Supervision; Investigation; Data curation; Writing- review & revise
N. Shaw: Investigation; Data curation; Writing & editing - original draft

Availability of Data and Materials
The data supporting the findings of this study are available upon request from the corresponding author.

Ethics Statement
This study did not involve human participants or animals. Therefore, ethical approval was not required.

Generative Artificial Intelligence Declarations
The authors claim that artificially intelligent-assisted technologies, such as generative AI, were not used to generate content, ideas, or theories. We have just utilized AI to enhance readability and refine the language. This was done with extreme human control and oversight. The authors take full responsibility for reviewing and approving the content.

References
[1] H. Ramakrishnan, R. Balasundaram, N. Ganesh, and N. Karthikeyan, "Experimental investigation of cut quality characteristics on SS321 using plasma arc cutting," *Journal of the Brazilian Society of Mechanical Sciences and Engineering*, vol. 40, no. 2, p. 60, 2018. https://doi.org/10.1007/s40430-018-0997-8.

[2] S. A. Hamood and V. N. Najm, "Optimization of plasma cutting parameters on dimensional accuracy and machining time for low carbon steel," *Engineering and Technology Journal*, vol. 38, no. 8A, pp. 1160–1168, 2020. https://doi.org/10.30684/etj.v38i8A.1151.

[3] P. Sawdatkar, V. Parmar, and D. Singh, "Review of plasma arc cutting process and its comparative analysis with laser beam machining process in terms of energy consumption," *Materials and Manufacturing Processes*, vol. 39, no. 9, pp. 1163–1186, 2024. https://doi.org/10.1080/10426914.2024.2362620.

[4] P. H. Agarwal and K. R. Patel, "Optimizing plasma arc cutting parameters for structural steel using grey relational analysis," *International Journal of Engineering Research & Technology*, vol. 8, no. 1, pp. 27–30, 2019.

[5] M. Field, J. F. Kahles, and W. P. Koster, "Surface finish and surface integrity," in *Machining. Materials Park*, OH, USA: ASM International, 1989, pp. 19–36.

[6] K. Rana, P. Kaushik, and S. Chaudhary, "Optimization of plasma arc cutting by applying Taguchi method," *International Journal of Enhanced Research in Science, Technology & Engineering*, vol. 2, no. 7, pp. 106–110, 2013.

[7] S. Naganathan, G. Jayaprakash, M. Thilak, and D. Manikandan, "Enhanced plasma arc machining performance for improved surface characteristics of SS304 using nickel nano-coated copper nozzle," *Surface Engineering*, p. 02670844251412168, 2026. https://doi.org/10.1177/02670844251412168.

[8] C. L. dos Santos, R. B. D. Pereira, C. H. Lauro, and L. C. Brandão, "Analysis of the cutting and forming tapping in holes produced by plasma cutting and helical drilling," *The International Journal of Advanced Manufacturing Technology*, pp. 1–13, 2026. https://doi.org/s00170-026-17629-1.

[9] S. Chabert, J. J. Gonzalez, and P. Freton, "Plasma arc cutting—Reversed swirl ring, electrode thread, and cut direction effects on kerf geometry," *Plasma Physics and Technology*, vol. 10, no. 1, pp. 1–4, 2023. https://doi.org/10.14311/ppt.2023.1.1.

[10] G. Singh and S. Akhai, "Experimental study and optimisation of MRR in CNC plasma arc cutting," *International Journal of Engineering Research and Applications*, vol. 5, no. 6, pp. 96–99, 2015.

[11] S. S. Sonu and S. Singla, "A review on optimization of influence parameters of EN-45A material using plasma arc cutting machine," *International Research Journal of Engineering and Technology*, vol. 8, no. 7, 2021.

[12] A. Rzeźnikiewicz, J. Górka, and M. Przybyła, "The air plasma cutting quality of selected construction materials," *International Journal of Modern Manufacturing Technologies*, vol. 15, no. 1, pp. 18–24, 2023. https://doi.org/10.54684/ijmmt.2023.15.1.18

[13] P. T. Hang, N. T. Chau, A. D. Khang, N. H. Anh, and P. H. Son, "Investigation on the effect of cutting parameters in CNC plasma cutting of carbon steel," *Vietnam Journal of Agricultural Sciences*, vol. 3, no. 4, pp. 831–842, 2020. https://doi.org/10.31817/vjas.2020.3.4.06.

[14] R. Bhuvenesh, M. H. Norizaman, and M. A. Manan, "Surface roughness and MRR effects in manual plasma arc cutting machining," *International Journal of Industrial and Manufacturing Engineering*, vol. 6, pp. 131–134, 2012. https://doi.org/10.5281/zenodo.1062516

[15] S. Chamarthi, N. S. Reddy, M. K. Elipey, and D. R. Reddy, "Investigation and analysis of plasma arc cutting parameters on surface unevenness of Hardox 400 material," *Procedia Engineering*, vol. 64, pp. 854–861, 2013. https://doi.org/10.1016/j.proeng.2013.09.161.

[16] S. Kumar, "Experimental study on parameter optimization in CNC plasma arc cutting of AISI 206 steel using Taguchi approach," *International Journal of Technical Research and Science*, vol. 3, no. 6, pp. 198–205, 2018.

[17] S. Sharma, M. Gupta, R. Kumar, and N. S. Bindra, "Experimental analysis and optimization of process parameters in plasma arc cutting of EN-45A using Taguchi and ANOVA," *International Journal of Mechanical and Industrial Engineering*, vol. 11, no. 7, pp. 1387–1391, 2017.

[18] N. Shaw and S. Chakravarti, "Experimental investigation of material removal rate for various cutting profiles in plasma arc cutting," *Suranaree Journal of Science and Technology*, vol. 32, no. 4, p. 030348, 2025. https://doi.org/10.55766/sujst8016.

[19] A. Das, S. R. Das, J. P. Panda et al., "Machine learning-based modelling and optimization in hard turning of AISI D6 steel with AlTiSiN-coated carbide tool," *arXiv preprint*, arXiv:2202.00596, 2022.

[20] P. Hema and R. Ganesan, "Experimental investigations on SS304 alloy using plasma arc machining," *SN Applied Sciences*, vol. 2, no. 4, pp. 1–16, 2020. https://doi.org/ 10.1007/s42452-020-2350-y.

[21] B. Babu, R. S. Jayaram, and P. Saravanamuthukumar, "Machining parameter effects on MRR and surface roughness of Monel 400 using Taguchi method," *NeuroQuantology*, vol. 20, no. 8, p. 4781, 2022. https://doi.org/10.14704/nq.2022.20.8.NQ44504.

[22] M. A. Padmanaban, N. Baskar, N. Senthilkumar, and M. Seeman, "Optimization of HW-GTAW process parameters for joining austenitic stainless steel using historic data design and zebra algorithm," *International Journal of Interactive Design and Manufacturing*, vol. 19, no. 4, pp. 2587–2605, 2025. https://doi.org/ 10.1007/s12008-024-01879-y.

[23] S. Chakravarti, "Experimental and statistical analysis for optimizing thermal performance of fins in forced convection systems," *Journal of Thermal Analysis and Calorimetry*, vol. 150, pp. 10299–10310, 2025. https://doi.org/10.1007/s10973-025-14371-w.

[24] C. Hamzaçebi, P. Li, P. A. R. Pereira, and H. Navas, "Taguchi method as a robust design tool," in *Quality Control—Intelligent Manufacturing, Robust Design and Charts*. London, U.K.: IntechOpen, 2020, pp. 1–19. https://doi.org/10.5772/intechopen.94908.

[25] B. Bhattacharjee, P. Chattopadhyay, R. Kumar et al., "Plasma arc machining on different steel alloys: A progressive review," in *AIP Conference Proceedings*, vol. 3007, no. 1, p. 100029, 2024. https://doi.org/10.1063/5.0200305.

[26] M. R. Choudhury et al., "Optimization of process parameters in plasma arc cutting of commercial-grade aluminium plate," *High Temperature Materials and Processes*, vol. 43, no. 1, p. 20220329, 2024. https://doi.org/ https://doi.org/10.1515/htmp-2022-0329.

[27] M. Gostimirović, D. Rodić, M. Sekulić, and A. Aleksić, "An experimental analysis of cutting quality in plasma arc machining," *Advanced Technologies and Materials*, vol. 45, no. 1, pp. 1–8, 2020. https://doi.org/10.24867/ATM-2020-1-001

[28] Z. Cinar, M. Asmael, and Q. Zeeshan, "Developments in plasma arc cutting of steel alloys: A review," *Jurnal Kejuruteraan*, vol. 30, no. 1, pp. 7–16, 2018. https://doi.org/10.17576/jkukm-2018-30(1)-01.

[29] A. Mohan, S. Samsudeensadham, A. A. Kumar, and M. Kirubakaran, "Prediction of surface characteristics in plasma arc cutting using image processing and fuzzy logic," in *Materials, Design, and Manufacturing for Sustainable Environment*, Springer, 2021, pp. 331–343.

[30] A. Özek, U. Çaydaş, and E. Ünal, "A fuzzy model for predicting surface roughness in plasma arc cutting of AISI 4140 steel," *Materials and Manufacturing Processes*, vol. 27, no. 1, pp. 95–102, 2012. https://doi.org/10.1080/10426914.2011.577868.

[31] R. Rahmawati, S. Anis, and R. Rusiyanto, "Effect of cutting speed and material thickness on hardness and surface roughness of AISI 1045 steel using CNC plasma arc cutting," *Jurnal Dinamika Vokasional Teknik Mesin*, vol. 4, no. 2, pp. 93–98, 2019. https://doi.org/10.21831/dinamika.v4i2.27390.

Abbreviations

PAC	Plasma Arc Cutting
CNC	Computer Numerical Control
MRR	Material Removal Rate
R_a	Surface Roughness
ANOVA	Analysis of Variance
DOE	Design of Experiments
S/N	Signal-to-Noise Ratio
CAD	Computer-Aided Design
3D	Three-Dimensional
IS	Indian Standard
VDC	Volts Direct Current
DoE	Design of Experiment
OA	Orthogonal Array